Research Article

Multisource Fault Signal Separation of Rotating Machinery Based on Wavelet Packet and Fast Independent Component Analysis

Feng Miao [iD],[1] **Rongzhen Zhao** [iD],[2] **Leilei Jia,**[1] **and Xianli Wang**[1]

[1]*School of Physical and Electrical Information, Luoyang Normal University, Luoyang 471022, China*
[2]*Key Laboratory of Digital Manufacturing Technology and Application, The Ministry of Education, Lanzhou University of Technology, Lanzhou 730050, China*

Correspondence should be addressed to Feng Miao; miaofeng3699@163.com

The vibration signal of rotating machinery compound faults acquired in actual fields has the characteristics of complex noise sources, the strong background noise, and the nonlinearity, causing the traditional blind source separation algorithm not be suitable for the blind separation of rotating machinery coupling fault. According to these problems, an extraction method of multisource fault signals based on wavelet packet analysis (WPA) and fast independent component analysis (FastICA) was proposed. Firstly, according to the characteristic of the vibration signal of rotating machinery, an effective denoising method of wavelet packet based on average threshold is presented and described to reduce the vibration signal noise. In the method, the thresholds of every node of the best wavelet packet basis are acquired and averaged, and then the average value is used as a global threshold to quantize the decomposition coefficient of every node. Secondly, the mixed signals were separated by using the improved FastICA algorithm. Finally, the results of simulations and real rotating machinery vibration signals analysis show that the method can extract the rotating machinery fault characteristics, verifying the effectiveness of the proposed algorithm.

1. Introduction

Rotating machinery plays an increasingly important role in modern industry and intelligent manufacturing. The real-time monitoring of the working state of rotating machinery can not only avoid the occurrence of disasters but also increase obvious economic benefits [1, 2]. The rotor system is one of the important joints of rotating machinery equipment in industrial production. It is widely used in different fields. The normal operation of the rotor system is directly related to the working performance of the whole mechanical equipment. Therefore, the rotor system is a good research object of the exploration and mining of new fault diagnosis methods. In practical engineering, the rotor vibration signal caused by local defects usually has the characteristics of nonlinear, nonstationary, low signal-to-noise ratio, and unclear fault characteristics [3, 4]. It is difficult to make effective diagnosis by directly using spectrum analysis. In addition, some conventional diagnostic methods such as spectral kurtosis and time-frequency analysis have their own limitations.

Therefore, it is a practical problem to explore an effective fault diagnosis method for the rotor system in engineering practice [5, 6].

In order to effectively identify the feature information contained in the fault signal of rotating machinery and reveal its inherent characteristics, many fault feature extraction methods of rotating machinery have been proposed, such as empirical mode decomposition (EMD) [7, 8], mathematical morphology filtering [9, 10], wavelet decomposition [11, 12], adaptive filtering [13, 14], matching pursuit [15, 16], cyclostationary signal analysis [17, 18], Wiener filter [19], Kalman filter [20, 21], and stochastic resonance [22, 23] that are widely used in early fault diagnosis of rotating machinery. The EMD proposed by Huang et al. [7] is a nonstationary signal analysis method, which can find the hidden characteristic information in the signal, and has been widely used in the extraction and noise reduction of the impact signal of rotating machinery. Xin et al. [24] proposed a fault feature extraction and diagnosis method for vibration signal based on iterative empirical wavelet transform (EWT) and sparse filter

(SF). Pang et al. [25] proposed an adaptive filtering algorithm based on mathematical morphology for rolling bearing fault diagnosis. Kang et al. [20] proposed an improvement method associated with the Kalman filter to estimate the bearing dynamic coefficients. Cheng et al. [26] proposed a novel deconvolution algorithm called adaptive multipoint optimal minimum entropy deconvolution adjusted (AMOMEDA) for extracting fault-related features from noisy vibration signals. The condition monitoring and diagnosis technology of mechanical equipment has made many encouraging achievements and has been gradually applied to practice. However, there are still many problems in the research of fault diagnosis mechanism, signal detection, feature extraction, and fault reasoning, which need to be further studied. For example, the detection method of fault characteristic signal of rotating machinery is not universal. One of the important problems is that the working condition of the equipment is often complex, and the fault characteristic signal is often superimposed by various interference signals. How to effectively remove the interference signal and extract the effective signal has become a key problem. The emergence of blind signal separation (BSS) theory can provide a feasible way to solve the above problems. Blind signal separation refers to the process of recovering the source signal only from the observed signal according to the statistical characteristics of the source signal when the parameters of the source signal and transmission channel are unknown.

BSS plays an increasingly important role in the field of digital signal processing and has been widely used in communication [27], speech processing [28], fault diagnosis [29, 30], seismic exploration [31], biomedicine [32, 33], image processing [34], radar [35], and economic data analysis [36]. In blind signal separation, the typical algorithms commonly used include the fast fixed-point algorithm [37], natural gradient algorithm [38], Equivariant Adaptive Separation via Independence (EASI) algorithm [39, 40], and Joint Approximation Diagonalization of Eigen-matrices (JADE) algorithm [41, 42], etc. Grotas et al. [43] developed the constrained maximum likelihood (ML) estimator of the Laplacian matrix for this graph BSS problem with Gaussian-distributed states. Eitner et al. [44] used two blind source separation algorithms to estimate the modal parameters of a reduced-scale rocket nozzle using only measurements of deformation. Ge and Jiang [9] proposed a framework based on joint blind source separation (JBSS) in order to solve the jamming suppression problem in the noise environment for the distributed radar with single transmitter and multiple receivers, where the multiple jamming enter into all the receivers through the main beam of the antennas. Belaid et al. [45] proposed a new multiscale decomposition algorithm which enables the blind separation of convolutely mixed images. All the above algorithms show good separation performance when separating noiseless mixed signals. However, in the separation of noisy signals, there will be a large error, especially in the case of low signal-to-noise ratio, and even draw a completely wrong conclusion, because these algorithms are derived without considering the noise model. In the process of rotating machinery running, the signal mea-

sured by vibration sensor installed on mechanical equipment inevitably contains signal noise. If the noise is ignored and the blind source separation algorithm is directly used to separate the mixed vibration signals, it may produce large errors or draw wrong conclusions. Therefore, before the blind separation of mechanical vibration signals, it is very important to reduce the noise and improve the signal-to-noise ratio.

Therefore, aiming at the problem of weak fault feature signal extraction of rotating machinery under the influence of noise, a fault separation method based on wavelet packet analysis (WPA) filter and improved fast independent component analysis (FastICA) algorithm is proposed. Firstly, wavelet packet filter is used to denoise the mixed signal under noise interference, and then the improved FastICA algorithm is used to separate the denoised signal, and then the weak fault signal is effectively extracted.

The contents of the following sections are as follows: Section 2 introduces the basic theory and model of blind source separation. Section 3 presents the principle of the wavelet packet denoising algorithm. Section 4 presents implementation algorithm steps of the improved WPA-FastICA Method. Simulated and experimental verifications are conducted in Sections 5 and 6. Finally, the conclusions and outlook are both given in Section 7.

2. The Basic Theory and Model of Blind Source Separation

Blind source separation (BSS) refers to the process of extracting and recovering (separating) the original signals which cannot be directly observed from multiple observed mixed signals. The "blind" means that the source signal is unobservable, and the hybrid system characteristics are unknown or only a small amount of prior knowledge is known. Independent component analysis (ICA) is the main method to solve the problem of blind source separation, which is based on the independence of the source signal. The solution steps of ICA are as follows: establish the objective function of the observed signal according to the principle of statistical independence and then use the optimization algorithm to separate the observed signal, so that the output component is as independent or completely independent as possible in statistics. In this way, the signal can be separated.

The mathematical model of fast ICA problem is described as follows:

$$x_i = \sum_{j=1}^{n} a_{ij} s_j(t) + n_i(t) \, ; i = 1, 2, 3, \cdots, m, \qquad (1)$$

where $x(t) = [x_1(t) x_2(t) \cdots x_m(t)]^T$ is the observation signal with m-dimension, A is the mixing matrix of source signal aliasing and unknown, $s(t) = [s_1(t) s_2(t) \cdots s_n(t)]^T$ is the source signal, and $n(t) = [n_1(t) n_2(t) \cdots n_m(t)]^T$ is the noise.

It can be expressed as a vector

$$
\begin{pmatrix} x_1 \\ x_2 \\ x_3 \\ \vdots \\ x_m \end{pmatrix} = \begin{pmatrix} a_{11} & \cdots & a_{1n} \\ \vdots & \vdots & \vdots \\ a_{m1} & \cdots & a_{mn} \end{pmatrix} \begin{pmatrix} s_1 \\ s_2 \\ s_3 \\ \vdots \\ s_n \end{pmatrix} + \begin{pmatrix} n_1 \\ n_2 \\ n_3 \\ \vdots \\ n_n \end{pmatrix}. \tag{2}
$$

The purpose of fast ICA is to find a separation matrix W to separate the source signal $s(t)$ from $x(t)$, and the mathematical model of the separation process is expressed as follows:

$$
y(t) = Wx(t), \tag{3}
$$

which is

$$
\begin{pmatrix} y_1(t) \\ y_2(t) \\ y_3(t) \\ \vdots \\ y_m(t) \end{pmatrix} = Y = WX = WAS = GS = G \begin{pmatrix} s_1(t) \\ s_2(t) \\ s_3(t) \\ \vdots \\ s_n(t) \end{pmatrix}, \tag{4}
$$

Where $y(t)$ is the estimated value of $s(t)$. To separate the source signal is to find the separation matrix U to make the following true:

$$
\widehat{S}(t) = UX(t) = UA\tilde{S}(t). \tag{5}
$$

If

$$
UA = I, \tag{6}
$$

where if I is a unit matrix, then $\widehat{S}(t)$ is an effective separation of $\tilde{S}(t)$.

3. The Principle of the Wavelet Packet Denoising Algorithm

Wavelet packet analysis is a more detailed analysis and reconstruction method of signal from wavelet analysis. In wavelet analysis, the signal is actually decomposed into low-frequency rough parts and high-frequency details, and then only the low-frequency details are decomposed for the second time, instead of the high-frequency parts [46, 47]. But in practice, we are only interested in some undetermined time (point) or frequency domain (point) signal, only need to extract the information of these specific time and frequency points. In this case, the fixed distribution of the time-frequency window of orthogonal wavelet transform is not an optimal choice. Wavelet packet analysis not only decomposes the low-frequency part but also makes a secondary decomposition of the high-frequency part, which can make

a more detailed description of the high-frequency part of the signal, and has a stronger ability to analyze the signal.

In order to simplify the problem without losing generality, considering that the collected vibration signal contains noise signal and has statistical characteristics, and considering that the measured vibration signal data is discrete data in time, the equation for vibration signal is established as follows:

$$
x(t) = As(t) + n(t), \tag{7}
$$

where $x(t)$ is the sampling signal, A is the mixing matrix of source signal aliasing and unknown, $s(t)$ is the source signal, and $n(t)$ is the noise signal.

Suppose $\{h_n\}_{n \in z}$ is the orthogonal low-pass real filter corresponding to the orthogonal scaling function $\Phi(t)$, and $\{g_n\}_{n \in z}$ is the high pass filter corresponding to the orthogonal wavelet function $\Psi(t)$, where $g_n = (-1)^n h_{1-n}$; that is, the two coefficients satisfy the orthogonal relationship, and then the recursively defined function μ_n is called the wavelet packet determined by the orthogonal scaling function $\mu_0 = \Phi$. So, there is the following function:

$$
\begin{cases} \mu_{2n}(t) = \sqrt{2} \sum_{k \in z} h_k \mu_n(2t - k), \\ \mu_{2n+1}(t) = \sqrt{2} \sum_{k \in z} g_k \mu_n(2t - k), \end{cases}, (n = 1, 2, 3 \cdots). \tag{8}
$$

Therefore, for any nonnegative integer Nez, there exists the following equation:

$$
U_{j+1}^n = U_j^{2n} \oplus U_j^{2n+1}, (j \in z). \tag{9}
$$

If the orthogonal wavelet decomposition algorithm of the Mallat multiresolution analysis algorithm is extended to the wavelet packet decomposition algorithm, the fast decomposition and reconstruction formula of wavelet packet can be obtained. It is expressed as follows:

$$
\begin{cases} d_j^{2n}(k) = \sum_{l \in z} h_{l-2k} d_{j+1}^n[l], \\ d_j^{2n+1}(k) = \sum_{l \in z} g_{l-2k} d_{j+1}^n[l], \end{cases} \tag{10}
$$
$$
d_{j+1}^n(k) = \sum_{l \in z} h_{k-2l} d_j^{2n}[l] + \sum_{l \in z} g_{k-2l} d_j^{2n+1}[l],
$$

where the coefficients d_j^{2n} and d_j^{2n+1} are the projections of an approximation function $f(t)$ at scale 2^l on subspaces U_j^{2n} and U_j^{2n+1}, respectively. Therefore, wavelet packet decomposition can not only decompose the low-frequency components of the signal but also can decompose the high-frequency components. Figure 1 is the schematic diagram of wavelet packet decomposition, in which A represents low-frequency coefficients, D represents high-frequency coefficients, and numbers indicate the number of levels of wavelet packet decomposition.

(a) The time domain signals
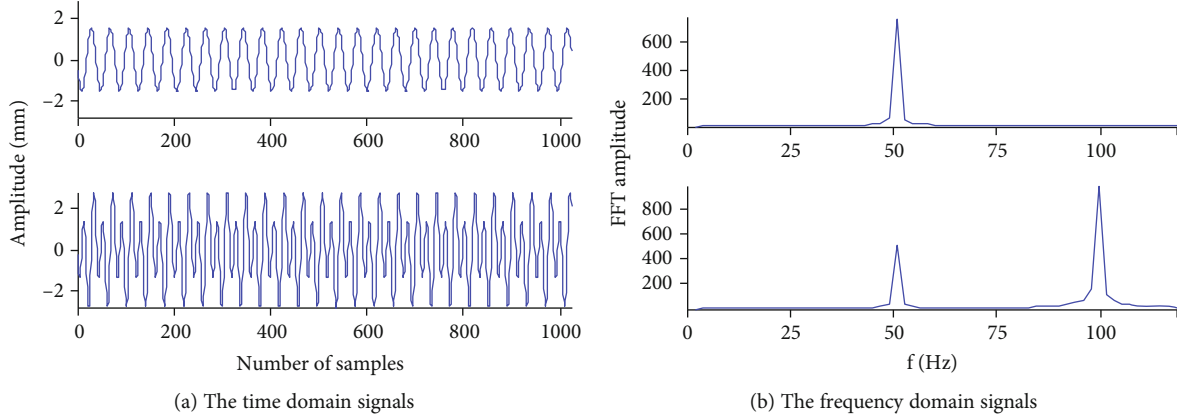
(b) The frequency domain signals

FIGURE 1: The time–frequency waveform of source signal.

A group of normal orthogonal bases extracted from wavelet library which can form $L^2(R)$ are called wavelet packet bases. Different wavelet packet bases have different abilities of time-frequency localization, and wavelet packet decomposition of a signal can be realized by many wavelet packet bases. Therefore, in order to better express the characteristics of signals, it is necessary to find an optimal wavelet packet basis. People usually define an information cost function that satisfies both additive and concentration properties to select the optimal wavelet basis. The common information cost functions include Shannon entropy, l^p norm ($1 \leq p \leq 2$), logarithmic energy entropy, and threshold entropy. The commonly used definition of Shannon entropy is as follows:

$$E(s_i) = -\sum_i s_i^2 \lg \left(s_i^2\right), \tag{11}$$

where $0 \lg (0) = 0$. According to these information cost functions, the wavelet packet sequence which minimizes the information cost function is obtained. The best wavelet packet basis can be obtained by using the fast search method from bottom to top.

In wavelet analysis, threshold denoising is a common method. Similarly, in wavelet packet analysis, the threshold method can also be used to process the coefficients of wavelet packet decomposition. In practice, how to select the threshold is the key to the algorithm design. The usual threshold selection is based on Donoho's hard threshold and soft threshold. The mathematical expression is as follows:

$$\mathrm{WH}_j = \begin{cases} \mathrm{sign}\left(\mathrm{WT}_{j,k}\right) \circ \left[\left|\mathrm{WT}_{j,k}\right| - \mu\lambda\right], & \left|\mathrm{WT}_{j,k}\right| \geq \lambda \\ 0, & \left|\mathrm{WT}_{j,k}\right| \leq \lambda \end{cases}, \tag{12}$$

Where $\mathrm{WT}_{j,k}$ is the wavelet decomposition coefficient before processing, sign $(\circ)$ is its symbol, WH_j is the coefficient after processing, $1 \prec j \prec J$, J is the maximum number of layers of wavelet decomposition, λ is the threshold value, when $\mu = 0$, and it is the hard threshold method; when $\mu = 1$, it is the soft threshold method.

Generally, the threshold selection criteria include unbiased likelihood estimation, fixed threshold criterion, hybrid criterion, and minimax criterion. Here, the threshold AA is selected as

$$\lambda = \sigma\sqrt{2 \lg (N)}, \tag{13}$$

where N is the number of high-frequency coefficients in the corresponding decomposition level, and σ is the noise standard deviation. Generally, its value is the median value of the absolute value of wavelet packet decomposition coefficient $WT_{j,k}$ in each layer divided by 0.6745. The formula can be expressed as follows:

$$\sigma = \mathrm{median}\left(\left|\mathrm{WT}_{j,k}\right|\right)/0.6745, \tag{14}$$

where median$(\circ)$ is the median value. In addition, soft threshold denoising can be divided into global threshold denoising and layered independent threshold denoising. The global threshold means that the same threshold is used to process each layer coefficient of wavelet packet decomposition, while the layered independent threshold means that different thresholds are used when processing each layer coefficient. The results show that the global denoising threshold value is better than the independent threshold value.

In this paper, an average threshold method is proposed to extract the vibration signal of rotating machinery. Firstly, the noise standard deviation of each node after wavelet packet decomposition is obtained by using formula (14), and the threshold value of each node is calculated by formula (13). Then, the threshold value of all nodes is averaged as the global threshold of wavelet packet denoising. The formula can be expressed as follows:

$$\lambda = \frac{1}{M}\sum_{m-1}^{M} \sigma_m \sqrt{2 \lg (N)}, \tag{15}$$

where $1 \prec m \prec M$, M, is the number of nodes after wavelet packet decomposition, $1 \prec j \prec J$.

Therefore, according to the wavelet packet analysis method, the following steps can be adopted to filter the noisy

signal collected by the sensor. The specific algorithm steps are as follows.

Step 1. The level n of wavelet packet decomposition is determined, and the vibration signal of rotating machinery under strong background noise is decomposed by wavelet packet.

Step 2. Shannon entropy is chosen as the information cost function to determine the optimal orthogonal wavelet packet basis.

Step 3. For the coefficients on each node of the optimal wavelet packet basis, the average threshold is obtained according to formula (15), and the threshold is processed by using the soft threshold method.

Step 4. The coefficients of the optimal wavelet packet basis after thresholding are reconstructed to realize the filtering of weak vibration signal under strong noise background.

4. The Algorithm of Blind Source Separation

4.1. Problem Description of Blind Source Separation. The ICA method is a kind of signal processing method to extract independent signal sources when the observed data are known and the mixing mode of signal sources is unknown. This method takes the non-Gaussian source signals as the research object, and under the assumption of their statistical independence, blind separation is carried out for the multichannel observed mixed signals, so as to separate the independent source signals hidden in the mixed signals perfectly The classical ICA model is as follows:

$$X(t) = AS(t), \qquad (16)$$

where X is the m-dimensional observation signal; S is the n-dimensional source signal; A is the $M \times N$ mixed matrix, which is generally assumed to be $M = N$.

By inverse equation (16), we can get the following results:

$$Y = WX, \qquad (17)$$

where Y is the estimation of source signal S and $W = A^{-1}$ is the unmixing matrix.

The basic idea of ICA is to adjust the weight vector w_i to make the components of the output signal y_i as independent as possible. In this paper, the FastICA algorithm with simple calculation and fast convergence speed is used to extract the source signal.

The iterative formula of the separation matrix is as follows:

$$
\begin{aligned}
w_i^+ &= E\left[Zg\left(w_i^T Z\right)\right] - E\left[Zg'\left(w_i^T Z\right)w_i\right], \\
w_i &= w_i / \|w_i^+\|.
\end{aligned}
\qquad (18)
$$

In the formula, Z is the whitened signal of the observation signal X; the nonlinear function is $g(u) = u \exp\left(-au^2/2\right)$, and $a = 1$.

In practice, the observed signal is often mixed with various noises. The model is as follows:

$$X(t) = AS(t) + N(t), \qquad (19)$$

where $N(t)$ is the additive white Gaussian noise; so, the estimated $Y = \widehat{S} + v$ is the noisy signal, where $\widehat{S}$ is the unbiased estimation of S; v is the noise signal. When it is sparse, the standard ICA model can carry out sparse coding of uncorrelated components and then select the contraction function to remove the noise in it. The probability density function model of the signal needs to be selected. In this paper, the double exponential function is selected to approximate the fault signal. The function is as follows:

$$p(Y) = \frac{1}{\sqrt{2}} \exp\left(-\frac{\sqrt{2}}{d}|Y|\right), \qquad (20)$$

where $p(Y)$ is the sparse distribution and $d = E[Y^2]$ is the scale value.

$\widehat{S}$ can be obtained by maximum likelihood estimation as follows:

$$\widehat{S} = f(WX), \qquad (21)$$

where f is the contraction function, which is defined as

$$f(Y) = \text{sign}\,(Y) \max\left\{0, |Y| - \sqrt{2}\sigma^2\right\}, \qquad (22)$$

where σ^2 is the variance of the signal containing noise.

4.2. Algorithm Steps of the Improved WPA-FastICA Method. In this paper, the specific steps of the multisource weak signal extraction method are as follows:

$$Z = \left[z_1 z_2 \cdots z_p\right]^T. \qquad (23)$$

Step 1. Using sensor to collect p-channel linear aliasing noise observation signal $X = [x_1 x_2 \cdots x_p]$. The wavelet packet decomposition of each observation signal x_i is to use $db2$ as the wavelet basis function to decompose the noisy signal in five layers and use Shannon entropy to get the reconstructed denoised signal.

Step 2. The denoised signal $x_i'(t)$ is deaveraged to make $E[x_i'(t)] = 0$ and then whitened to obtain the signal z_i. The p-path signal in X' is obtained after deaveraging and whitening.

Step 3. Let p be equal to the number of independent source signals to be estimated.

Step 4. The initial weight vector w_i is generated randomly, so that $w_i = w_i / \|w_i\|$.

Step 5. $w_i \leftarrow E[Zg(w_i^T Z)] - E[g'(w_i^T Z)]w_i, w_i = w_i / \|w_i\|$.

Step 6. Orthogonal normalization: $w_i \leftarrow w_i - \sum_{j=1}^{i-1}(w_i^T w_j)w_j$, $w_i = w_i/\|w_i\|$.

Step 7. If w_i does not converge, return to step (5).

Step 8. If w_i converges, then $i = i + 1$. If $i \leq p$, return to step (4).

Step 9. The solution matrix is $W = [w_1 w_2 \cdots w_p]^T$, and according to $Y = WZ$, the unmixing signal is $Y = [y_1 y_2 \cdots y_p]^T$.

Step 10. $\widehat{S}$ is calculated from equation (21), and pseudoinverse transformation is performed: $\widehat{S} = pinv(W)f(Y)$.

Finally, the separation signal is $\widehat{S} = [s\wedge_1 s\wedge_2 \cdots s\wedge_p]^T$.

5. Simulation

5.1. Evaluation Index of Separation Performance of the Method.
In the fast ICA algorithm, the main indexes to evaluate the separation performance of the algorithm usually include correlation coefficient, normalized mean square error (NMSE), and scatter plot of source signal and separated signal. At the same time, when the separation results with the same accuracy are obtained, the number of iterations is compared to evaluate the performance of the three algorithms.

5.1.1. Correlation Coefficient.
It describes the parameters of correlation between two signals. Suppose that the i-th signal in the source signal s is s_i, and the estimated signal obtained after the algorithm is run is s'_i, then the calculation formula of the correlation coefficient between s_i and s'_i is as follows [48]:

$$\rho = \frac{\text{cov}\left(s_i, s'_i\right)}{\sqrt{\text{cov}\left(s_i, s_i\right)\text{cov}\left(s'_i, s'_i\right)}}, \quad (24)$$

where $\text{cov}\left(\cdot\right)$ is the variance.

The closer the absolute value of the correlation coefficient between the two signals is 1, the closer the signal is, the better the separation effect of the algorithm is.

5.1.2. Normalized Mean Square Error (NMSE).
Normalized mean square error measure is used to measure the accuracy of hybrid matrix estimation. Its expression is as follows [49]:

$$\text{NMSE} = 10 \times \lg\left(\frac{\sum_{m=1}^{M}\sum_{n=1}^{N}(a\wedge_{mn} - a_{mn})^2}{\sum_{m=1}^{M}\sum_{n=1}^{N}(a_{mn})^2}\right)(dB). \quad (25)$$

In equation (18), M is the number of rows of A, N is the number of columns of A, and $\widehat{a}_{mn}$ is the estimated mixed matrix element. The smaller the value of NMSE, the higher the accuracy of mixed matrix estimation.

5.1.3. Number of Iterations.
It refers to the number of times that the formula in the algorithm is repeatedly calculated in order to approximate the desired target or result. When the ideal results can be obtained, the less iterations, the shorter the running time and the faster the convergence speed.

5.2. Simulation of Mixed Signal Separation under Different Carrier Frequencies and Noises.
In order to effectively simulate the fault characteristics of rotating machinery, the fault signal features under the actual working conditions of rotating machinery are selected to simulate the unbalance and rub impact faults. The simulation functions of these four types of source signals are as follows:

$$S(t) = \begin{Bmatrix} s_1(t) \\ s_2(t) \end{Bmatrix} = \begin{Bmatrix} 1.5\sin(100\pi t) \\ \cos(100\pi t) + 2\sin(200\pi t) \end{Bmatrix}, \quad (26)$$

where $s_1(t)$ simulates the unbalance fault signal and $s_2(t)$ simulates the characteristic signal of rub impact fault.

A mixing matrix $A \in R^{4 \times N}$ is generated randomly, and the two source signals are mixed according to equation (6).

$$X = As = A[s_1, s_2, s_3, s_4], \quad (27)$$

where X is the observable mixed signal and A is the mixing matrix, where

$$A = \begin{bmatrix} 0.311 & 0.673 \\ 0.926 & 0.176 \end{bmatrix}. \quad (28)$$

The time-frequency waveform of the mixed signal generated by matrix a mixing is shown in Figure 2; the time-frequency waveform of two source signals is shown in Figure 1.

It can be seen from Figure 1 that the simulated unbalance and rub impact fault signals are concentrated at 50 kHz and 100 kHz, respectively. Therefore, when wavelet packet is used for noise reduction, $db2$ wavelet is selected for 5-layer wavelet packet decomposition, and the second to sixth characteristic wavelet packet is selected for reconstruction, and the signal with frequency of 42.5-127.5 Hz is obtained as wavelet packet denoising signal. The interference noise $N(t)$ is generated automatically by MATLAB.

5.3. Result Analysis.
In order to compare with other separation methods, we add classic FastICA and SOBI separation methods to separate mixed signals and compare with WPA-FastICA method proposed in this paper.

The multisource unbalance and rub impact fault signals mixed with different intensities of white Gaussian noise are separated by using the extraction method in this paper. The source signals are mixed by random matrix, and then 0 dB, 10 dB, and 20 dB random white Gaussian noises are added, respectively, to obtain the observation signal shown in Figure 3. In order to intuitively compare the characteristics of the vibration signals before and after separation, it is necessary to analyze and compare the spectrum characteristics of the separated vibration signals under different noises.

Figure 4 is the time-frequency waveform after separating the simulation aliasing fault signal by using the classic
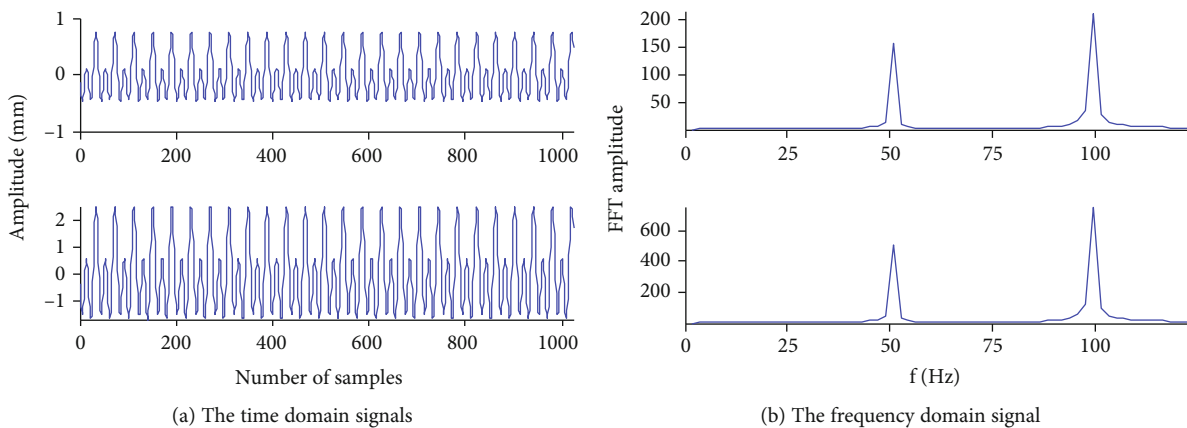
(a) The time domain signals

(b) The frequency domain signal

FIGURE 2: The time–frequency waveform of mixed signal.

(a) The time domain signals

(b) SNR = 0 dB

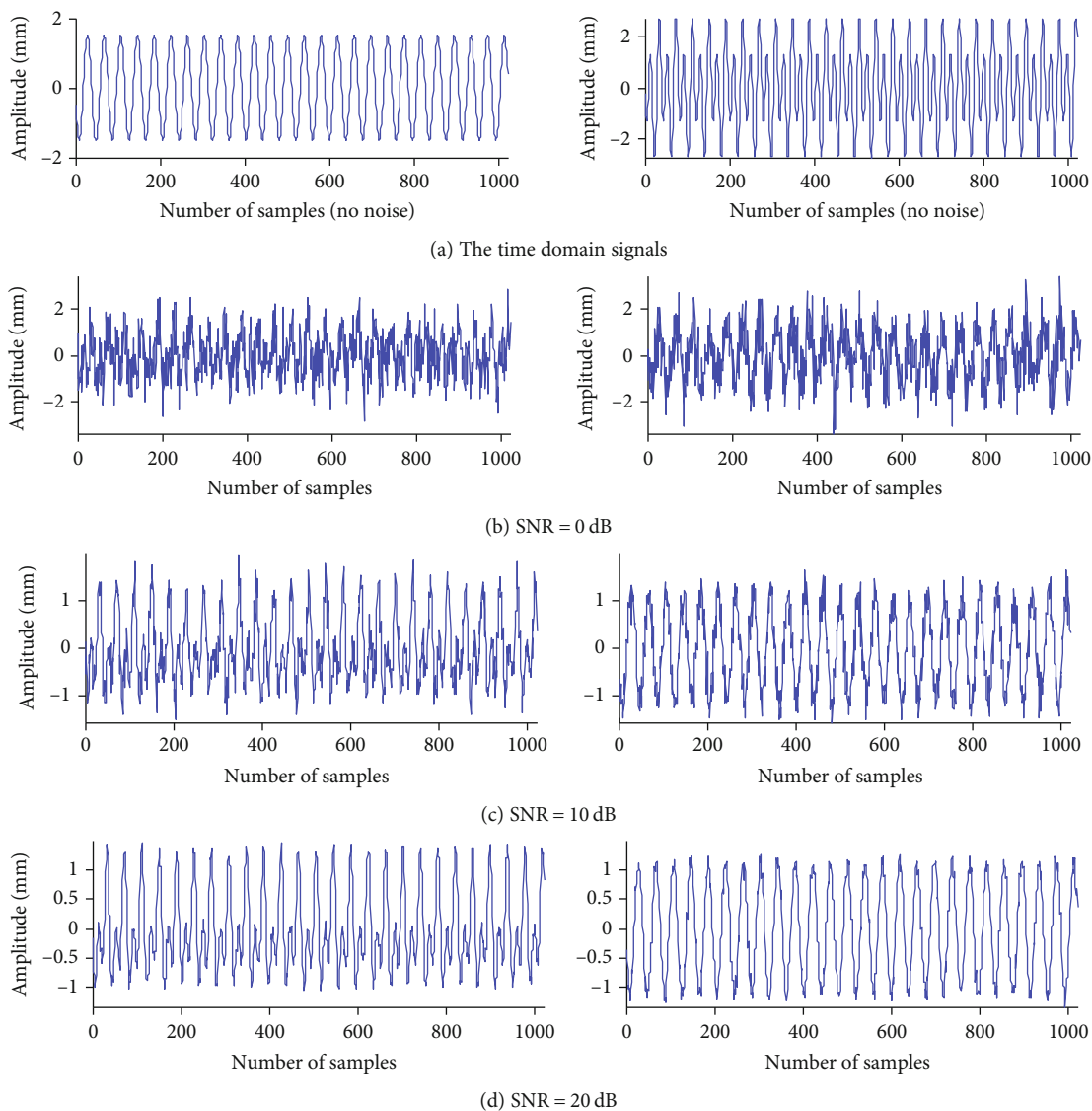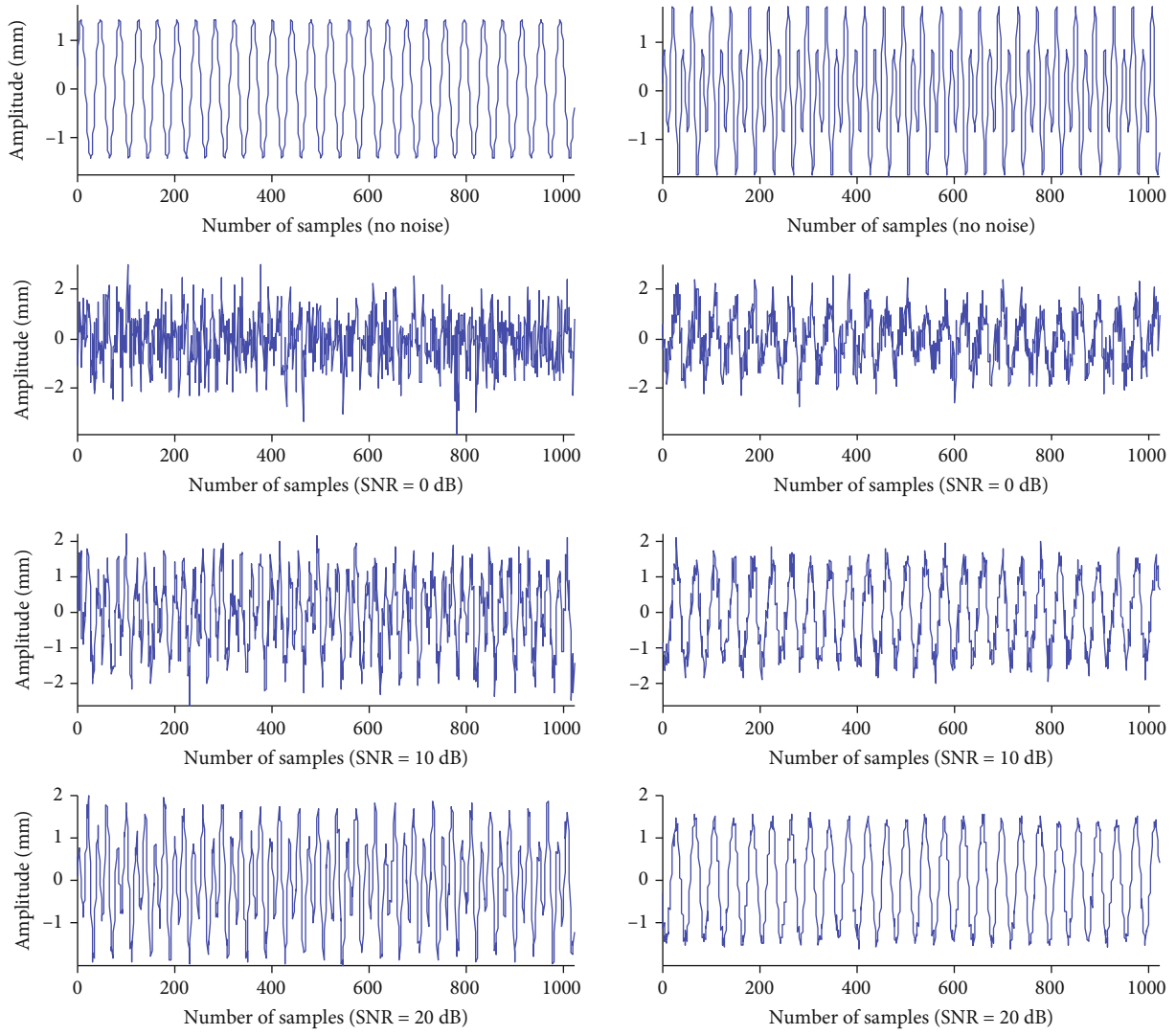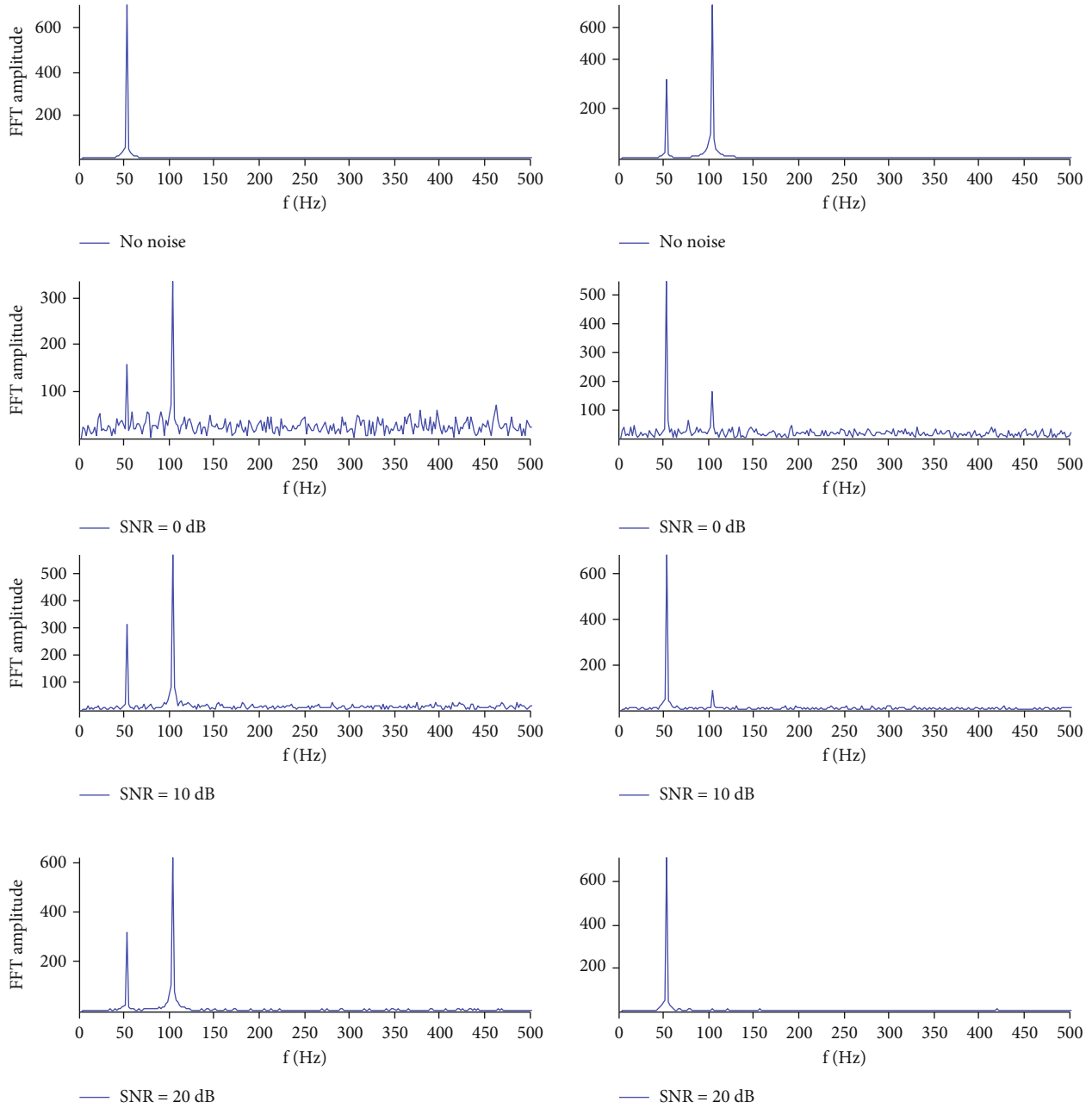(c) SNR = 10 dB

(d) SNR = 20 dB

FIGURE 3: Noisy signals with different input SNRs.

(a) The separated time domain signals with different noises by FastICA

FIGURE 4: Continued.

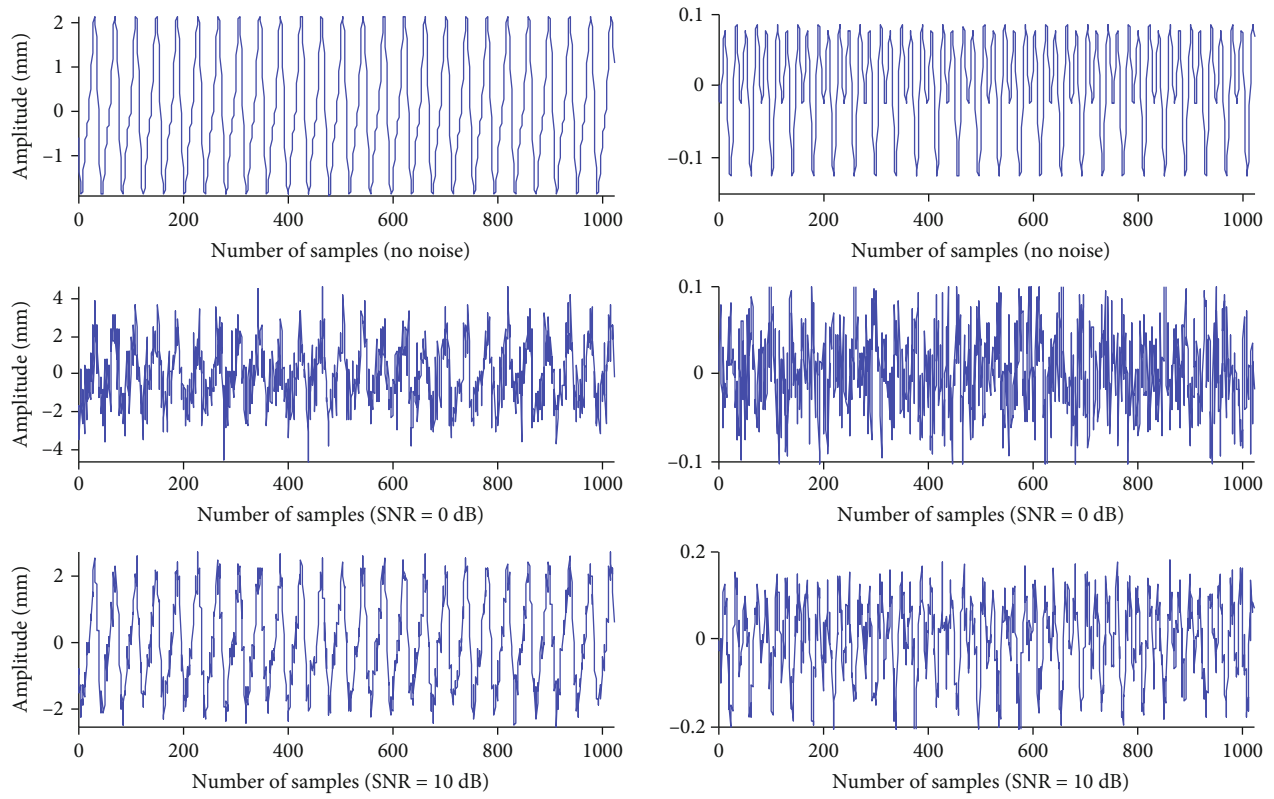(b) The separated frequency domain signals with different noises by FastICA

FIGURE 4: Time-frequency waveforms of the FastICA algorithm.

FastICA algorithm. It can be seen from Figure 4 that the classical FastICA algorithm has a very good separation effect when the signal-to-noise ratio is greater than 20, but when the signal-to-noise ratio is less than 20, the separation result is wrong. Figure 5 is the time-frequency waveform after separating the simulation aliasing fault signal by using the classical SOBI algorithm. It can be seen from Figure 5 that the separation result of the classical SOBI algorithm is wrong no matter under any Gaussian noise interference.

It can be seen from the time-domain waveform in Figure 6 that the algorithm proposed in this paper is used to separate the sampled signal under different noise interfer-

ence, and the noise can be well filtered from the time-domain waveform. Through the analysis of the frequency domain waveform characteristics, rub impact and unbalance fault can also be clearly identified when the signal-to-noise ratio is 0. The simulation fault is consistent with the separated fault signal, which shows that the WPA-FastICA algorithm can be used to separate the coupling faults of the rotor system.

Therefore, through Table 1 and Figures 4–6, compared with the three methods, the extraction effect of the proposed method is obviously better than that of the other two methods, and the direct separation by the SOBI method has the worst effect.

(a) The separated time domain signals with different noises by SOBI

FIGURE 5: Continued.
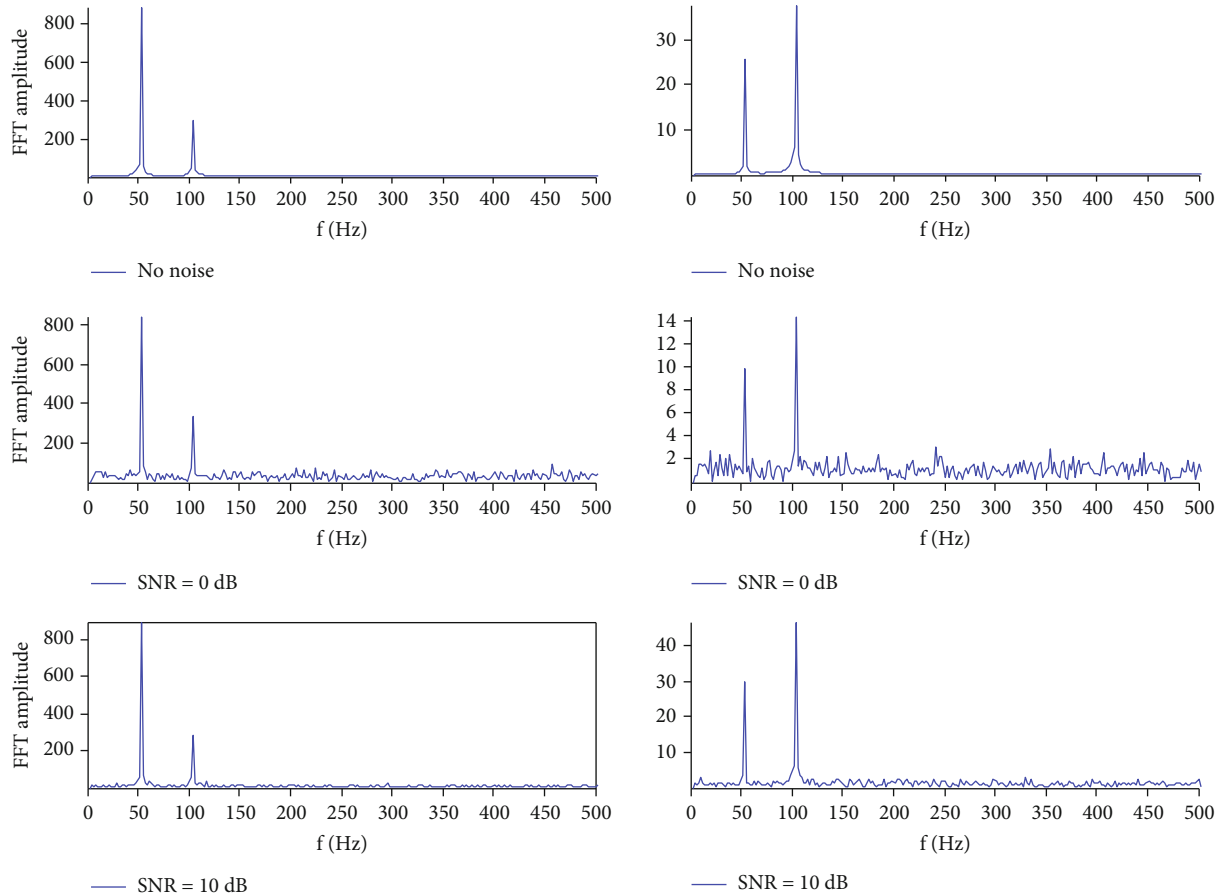
(b) The separated frequency domain signals with different noises by SOBI

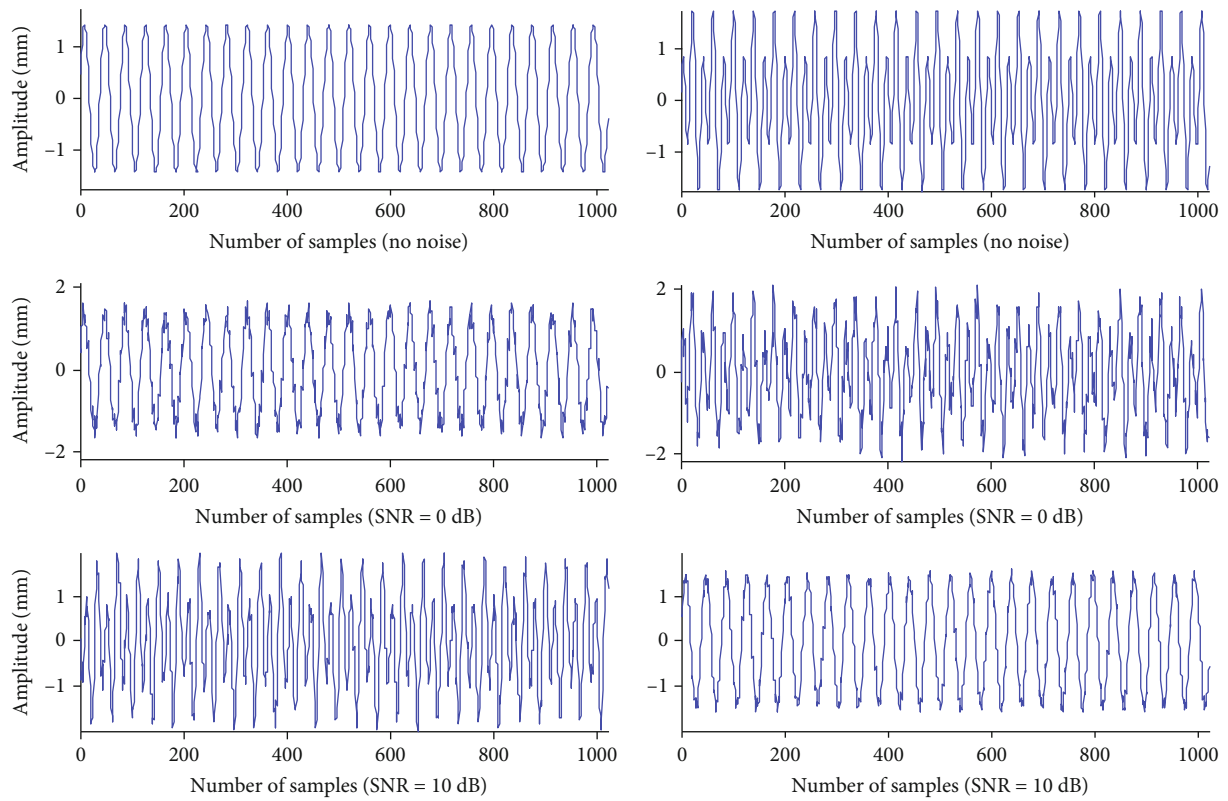Figure 5: Time-frequency waveform of the SOBI algorithm.

6. Applications

In order to effectively verify the effectiveness of the proposed method, a fault simulation experimental platform is built. The experimental table is shown in Figure 7(a). The experimental platform is 134 mm long, 51 mm wide, 120 mm high, and weighs about 50 kg. The rotor is composed of two shafts about 49 mm long and connected by coupling. There are three large mass disks and four small mass disks installed on the rotor, which are used to simulate the blades of rotating machinery in the industrial field. 13 sensors are installed on the bearing. The front 12 sensors are installed in the X direction and Y direction of the same section in a mutually perpendicular way, as shown in Figure 7(b). They are used to measure the vibration displacement signal of the rotor. After the vibration signals output by the sensors in the X and Y directions are combined, the rotor axis trajectory diagram of this section can be obtained. In the experimental process, the inverter is used to control the operation of the variable frequency motor, and then the rotor is driven by the variable frequency motor, and the motor power is about 1.1 KW. The minimum speed of the test bed can be set arbitrarily, and the maximum speed can reach 12000 rpm, which is far more than the critical speed of the system, which can

meet the experimental requirements. Moreover, the speed up and down of the rotor can be adjusted through the keyboard of the frequency converter. The control mode of the motor can be manual control or computer control.

The rotor test bed is an experimental device used to simulate the vibration of rotating machinery. Various rotor fault simulation experiments can be done on the rotor test bench, such as rotor misalignment, imbalance, pedestal looseness, dynamic and static rubbing, oil film whirl, and oil film oscillation. In addition, it can also be used for lubrication theory, nonelectric measurement, data acquisition, signal analysis, rotor bearing system dynamics, condition monitoring, and fault diagnosis. In this experiment, by adding bolts on the mass disk of the rotor test bed and adding rubbing device on the bearing, the simulation experiment of rotor unbalance and dynamic static rubbing fault is realized. The experimental speed is 3000 rd/min, and the sampling frequency is 5000 Hz.

The time-frequency waveform of rotor vibration signal collected by two sensors is shown in Figure 8. The classical second-order blind identification (SOBI) and separation algorithm are used to separate the sampled signal directly, and the time-frequency waveform of the separated signal is shown in Figure 9. The classical fast independent component analysis (FastICA) algorithm is used to separate the sampled

(a) The separated time domain signals with different noises by WPA-FastICA

FIGURE 6: Continued.
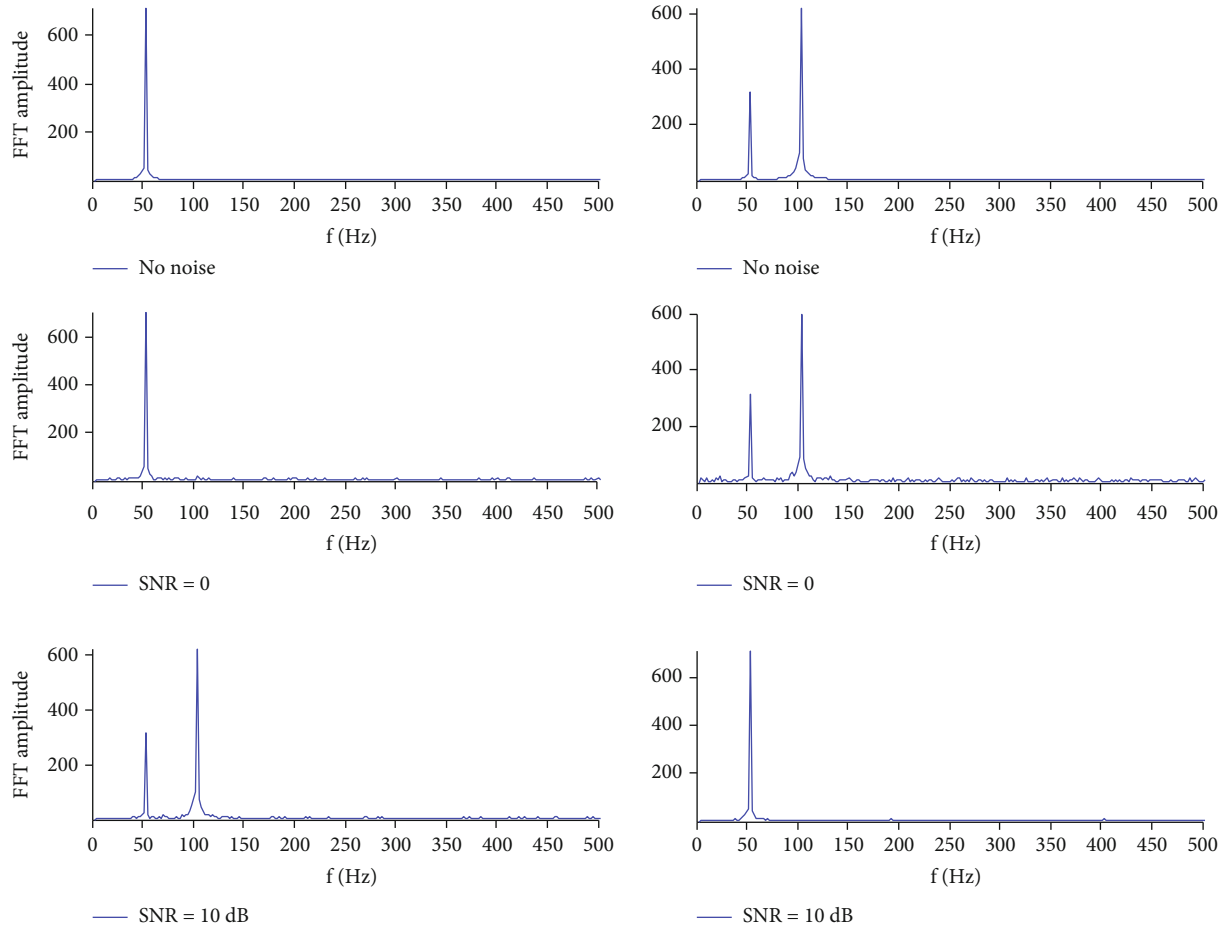
(b) The separated frequency domain signals with different noises by WPA-FastICA

FIGURE 6: Time-frequency waveforms signals of the WPA-FastICA algorithm.

TABLE 1: Comparison of evaluation indexes of blind source separation at SNR 0 dB.

Algorithm	s_i	ρ_i	NMSE/dB	t/s
SOBI	s_1	0.531	−12.142	
	s_2	0.611	−11.311	0.051
FastICA	s_1	0.911	−21.132	
	s_2	0.835	−21.214	0.043
WPA-FastICA	s_1	0.998	−52.212	
	s_2	0.997	−52.318	0.053

signal directly, and the time-frequency waveform of the separated signal is shown in Figure 10. The WPA-FastICA algorithm proposed in this paper is used to separate the sampled signal directly, and the time-frequency waveform of the separated signal is shown in Figure 11.

It can be seen from the time domain waveform in Figure 8 that the sampled signal is interfered by strong noise, and the fault characteristics of the rotor system cannot be identified from the time domain. However, from the characteristics of the frequency domain signal, we can clearly see the first harmonic of 50 Hz and the weak second harmonic of 100 Hz. From the analysis of frequency domain characteristics, only slight unbalance fault can be identified.

As can be seen from the time-domain waveform in Figure 9, the time-domain waveform separated by the classical SOBI algorithm contains strong noise; so, the fault characteristics of the rotor system cannot be identified from the time-domain waveform. However, from the characteristics of frequency-domain signals, it is obvious that one of the signals contains the first harmonic of 50 Hz and the second harmonic of 100 Hz, and the other signal is random and disordered. From the analysis of frequency domain characteristics, only slight unbalance fault can be identified.

It can be seen from the time-domain waveform in Figure 10 that under strong noise interference, the classical FastICA is used to directly separate the sampling signal, and the fault type of the rotor system cannot be identified from the time-domain waveform. However, through the frequency domain waveform characteristics, rub impact and unbalance fault can be identified, but the noise interference is particularly obvious.

As can be seen from the time-domain waveform in Figure 11 that under the strong noise interference, the algorithm proposed in this paper is used to separate the sampled signal. From the time-domain waveform, it can be seen that the noise
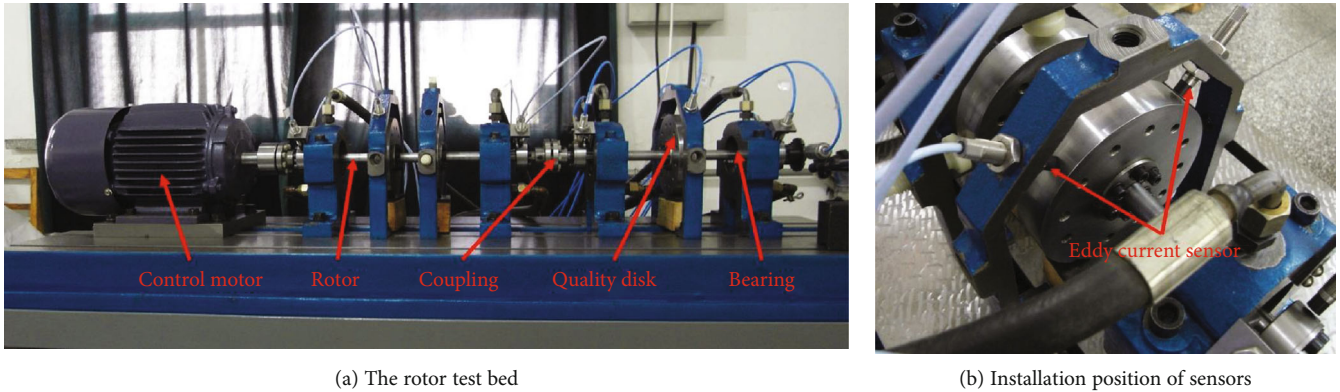
(a) The rotor test bed

(b) Installation position of sensors

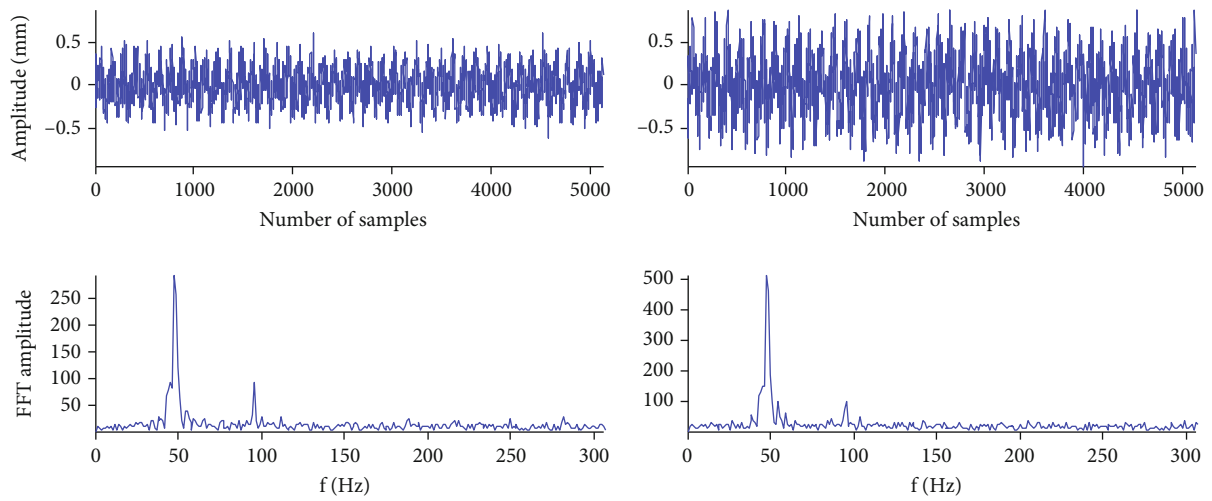FIGURE 7: Multifunctional rotor test platform.

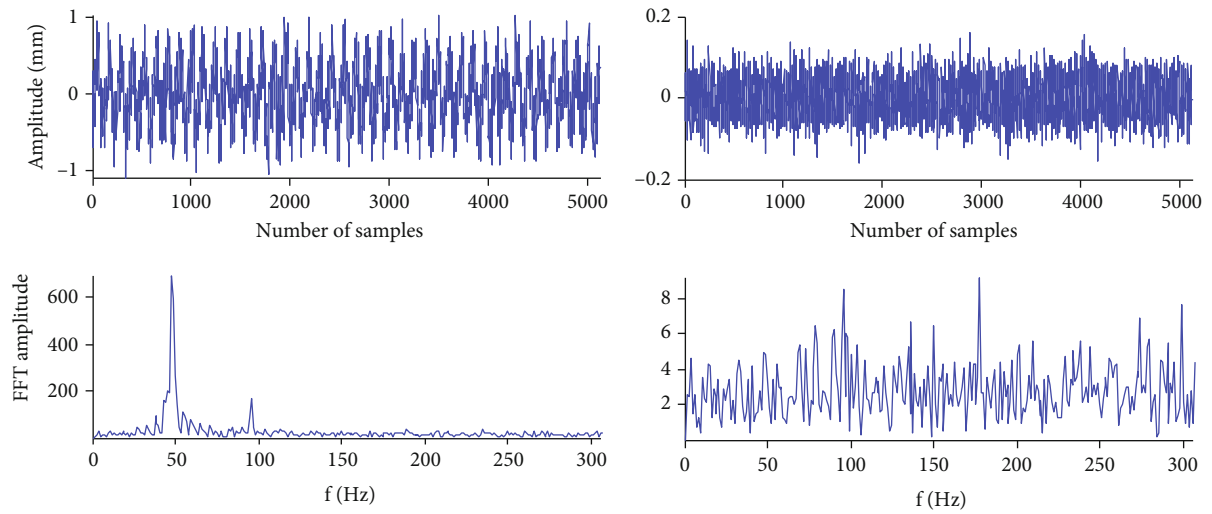FIGURE 8: Time frequency domain waveform of rotor coupling fault vibration signals.

FIGURE 9: Time–frequency waveforms of rotor coupling fault vibration signals by the SOBI algorithm.

is well filtered. According to the frequency domain waveform characteristics, rub impact and unbalance fault can be clearly identified. The simulated fault of the test bed is consistent with the separated fault signals, which shows that the WPA FastICA algorithm can be used to separate the coupling faults of the rotor system.
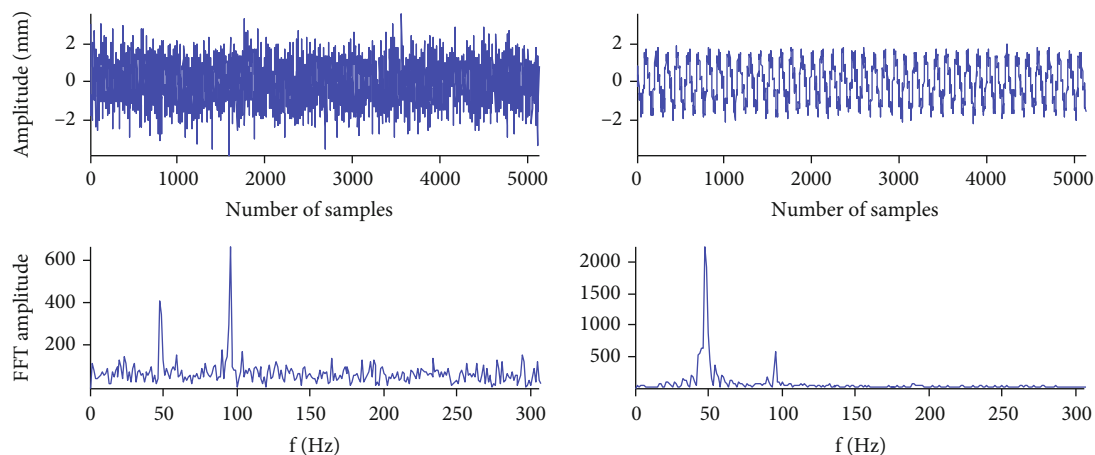
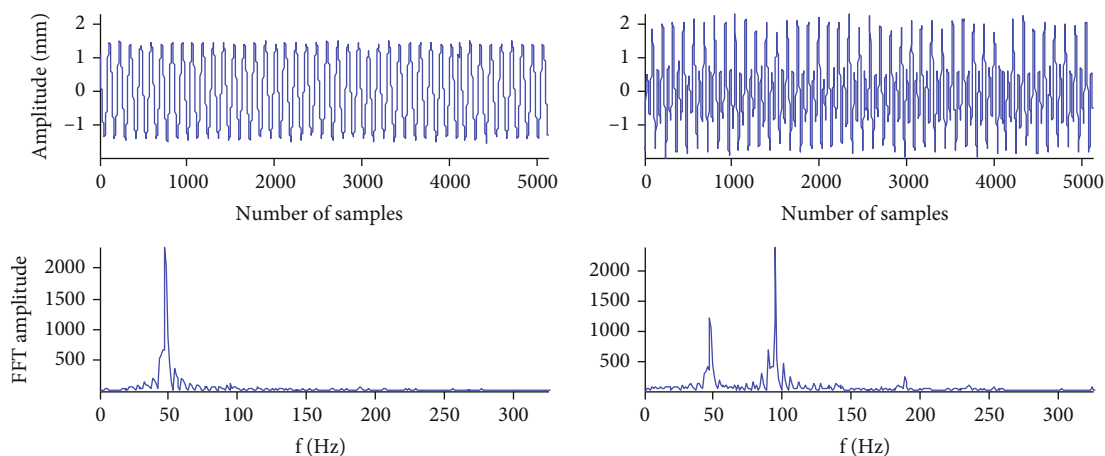FIGURE 10: Time–frequency waveforms of rotor coupling fault vibration signals by the FastICA algorithm.

FIGURE 11: Time–frequency waveforms of rotor coupling fault vibration signals by the WPA-FastICA algorithm.

7. Conclusions

A blind source separation algorithm based on WPA-FastICA is proposed to solve the problem of fast feature extraction for weak fault of rotating machinery. Our conclusions are as follows:

(1) In the background of noise interference, the vibration signal of rotating machinery has nonlinear and non-stationary characteristics, which will affect the effective extraction of fault features. In order to solve this problem, an algorithm combining wavelet packet filtering and blind source separation are introduced to effectively extract the components related to fault features, eliminate irrelevant components, and enhance the effective extraction of weak fault features

(2) If the traditional blind source separation (BSS) algorithm is used to separate the observed signals directly under noise interference, the separation result error is very different, especially when the signal-to-noise ratio is lower than 15 dB, even the wrong result may be obtained

(3) The improved WPA-FastICA blind source separation algorithm proposed in this paper can effectively separate the simulated rotor vibration signals, and its performance has been greatly improved compared with the traditional method under different noise interferences

(4) The improved WPA-FastICA blind source separation algorithm can separate the real rotor fault signal through the time and frequency domain analysis of the separated signal, which is consistent with the experimental set-up fault

Data Availability

The data used to support the findings of this study are included within the article.

Conflicts of Interest

The authors declare no conflict of interest.

Acknowledgments

References

[1] M. Rostaghi, M. R. Ashory, and H. Azami, "Application of dispersion entropy to status characterization of rotary machines," *Journal of Sound and Vibration*, vol. 438, pp. 291–308, 2019.

[2] F. Miao, R. Zhao, L. Jia, and X. Wang, "Fault diagnosis of rotating machinery based on Multi-Sensor Signals and Median Filter Second-Order Blind Identification (MF-SOBI)," *Applied Sciences*, vol. 10, no. 11, p. 3735, 2020.

[3] H. Shao, H. Jiang, H. Zhao, and F. Wang, "A novel deep autoencoder feature learning method for rotating machinery fault diagnosis," *Mechanical Systems and Signal Processing*, vol. 95, pp. 187–204, 2017.

[4] L. Song, H. Wang, and P. Chen, "Vibration-based intelligent fault diagnosis for roller bearings in low-speed rotating machinery," *IEEE Transactions on Instrumentation and Measurement*, vol. 67, no. 8, pp. 1887–1899, 2018.

[5] M. Xia, T. Li, L. Xu, L. Liu, and C. W. de Silva, "Fault diagnosis for rotating machinery using multiple sensors and convolutional neural networks," *Ieee-Asme Transactions on Mechatronics*, vol. 23, no. 1, pp. 101–110, 2018.

[6] H. Shao, H. Jiang, F. Wang, and H. Zhao, "An enhancement deep feature fusion method for rotating machinery fault diagnosis," *Knowledge-Based Systems*, vol. 119, pp. 200–220, 2017.

[7] N. E. Huang, M.-L. Wu, W. Qu, S. R. Long, and S. S. P. Shen, "Applications of Hilbert-Huang transform to non-stationary financial time series analysis," *Applied Stochastic Models in Business and Industry*, vol. 19, no. 3, pp. 245–268, 2003.

[8] R. Abdelkader, A. Kaddour, A. Bendiabdellah, and Z. Derouiche, "Rolling bearing fault diagnosis based on an improved denoising method using the complete ensemble empirical mode decomposition and the optimized thresholding operation," *IEEE Sensors Journal*, vol. 18, no. 17, pp. 7166–7172, 2018.

[9] Y. Ge and X. Jiang, "Mathematical morphology and deep learning-based approach for bearing fault recognition," *International Journal of Performability Engineering*, vol. 14, no. 5, pp. 995–1003, 2018.

[10] T. Gong, Y. Yuan, X. Yuan, and X. Wu, "Application of optimized multiscale mathematical morphology for bearing fault diagnosis," *Measurement Science and Technology*, vol. 28, no. 4, article 045401, 2017.

[11] Y. Liu, K. Li, and P. Chen, "Fault diagnosis for rolling bearings based on Synchrosqueezing wavelet transform," *Zhongguo Jixie Gongcheng/China Mechanical Engineering*, vol. 29, no. 5, pp. 585–590, 2018.

[12] G. Özmen and S. Özşen, "A new denoising method for fMRI based on weighted three-dimensional wavelet transform," *Neural Computing and Applications*, vol. 29, no. 8, pp. 263–276, 2018.

[13] C. Liu, Z. Zhang, and X. Tang, "Sign normalised spline adaptive filtering algorithms against impulsive noise," *Signal Processing*, vol. 148, pp. 234–240, 2018.

[14] M. A. Z. Raja, N. I. Chaudhary, Z. Ahmed, A. Ur Rehman, and M. S. Aslam, "A novel application of kernel adaptive filtering algorithms for attenuation of noise interferences," *Neural Computing and Applications*, vol. 31, no. 12, pp. 9221–9240, 2019.

[15] J. Li, M. Li, X. Yao, and H. Wang, "An adaptive randomized orthogonal matching pursuit algorithm with sliding window for rolling bearing fault diagnosis," *IEEE Access*, vol. 6, pp. 41107–41117, 2018.

[16] H. Wang and D. Sun, "The application of matching pursuit based on multi feature pattern set in the signal processing of rotating machinery," *Journal of Vibration and Control*, vol. 25, no. 13, pp. 1974–1987, 2019.

[17] Z. Ma, Y. Liu, D. Wang, W. Teng, and A. Kusiak, "Cyclostationary analysis of a faulty bearing in the wind turbine," *Journal of Solar Energy Engineering*, vol. 139, no. 3, 2017.

[18] A. Mauricio, J. Qi, and K. Gryllias, "Vibration-based condition monitoring of wind turbine gearboxes based on cyclostationary analysis," *Journal of Engineering for Gas Turbines and Power*, vol. 141, no. 3, 2019.

[19] L. Yu, J. Antoni, H. Wu, and W. Jiang, "Reconstruction of cyclostationary sound source based on a back-propagating cyclic wiener filter," *Journal of Sound and Vibration*, vol. 442, pp. 787–799, 2019.

[20] Y. Kang, Z. Shi, H. Zhang, D. Zhen, and F. Gu, "A novel method for the dynamic coefficients identification of journal bearings using Kalman filter," *Sensors*, vol. 20, no. 2, p. 565, 2020.

[21] M. C. Pan, W. C. Chu, and D.-D. Le, "Adaptive angular-velocity Vold-Kalman filter order tracking - Theoretical basis, numerical implementation and parameter investigation," *Mechanical Systems and Signal Processing*, vol. 81, pp. 148–161, 2016.

[22] P. Shi, C. Su, and D. Han, "Fault diagnosis of rotating machinery based on adaptive stochastic resonance and AMD-EEMD," *Shock and Vibration*, vol. 2016, Article ID 9278581, 11 pages, 2016.

[23] R. Jia, T. Li, Z. Xia, and X. Ma, "Vibration fault diagnosis of hydroelectric generating unit by using stochastic resonance and empirical mode decomposition," *Shuili Xuebao/Journal of Hydraulic Engineering*, vol. 48, no. 3, pp. 334–340, 2017.

[24] Y. Xin, S. Li, J. Wang, P. Yi, and J. Liu, "Gear fault diagnosis method based on iterative empirical wavelet transform," *Yi Qi Yi Biao Xue Bao/Chinese Journal of Scientific Instrument*, vol. 39, no. 11, pp. 79–86, 2018.

[25] B. Pang, G. Tang, Y. He, and T. Tian, "Weak fault diagnosis of rolling bearings based on singular spectrum decomposition, optimal Lucy-Richardson deconvolution and speed transform," *Measurement Science and Technology*, vol. 31, no. 1, article 015008, 2020.

[26] Y. Cheng, B. Chen, and W. Zhang, "Adaptive multipoint optimal minimum entropy deconvolution adjusted and application to fault diagnosis of rolling element bearings," *IEEE Sensors Journal*, vol. 19, no. 24, pp. 12153–12164, 2019.

[27] J. Lu, W. Cheng, Y. Zi, and Z. He, "Nonlinear blind source separation combining with improved particle swarm optimization," *Hsi-An Chiao Tung Ta Hsueh/Journal of Xi'an Jiaotong University*, vol. 50, no. 6, pp. 15–22, 2016.

[28] Y. Li, W. Nie, F. Ye, and Q. Wang, "A complex mixing matrix estimation algorithm in under-determined blind source separation problems," *Signal, Image and Video Processing*, vol. 11, no. 2, pp. 301–308, 2017.

[29] Y. Guo and A. Kareem, "System identification through nonstationary data using time-frequency blind source separation," *Journal of Sound and Vibration*, vol. 371, pp. 110–131, 2016.

[30] F. Miao and R. Zhao, "A new fault diagnosis method for rotating machinery based on SCA-FastICA," *Mathematical Problems in Engineering*, vol. 2020, Article ID 6576915, 12 pages, 2020.

[31] M. Kemiha and A. Kacha, "Complex blind source separation," *Circuits, Systems, and Signal Processing*, vol. 36, no. 11, pp. 4670–4687, 2017.

[32] F. Negro, S. Muceli, A. M. Castronovo, A. Holobar, and D. Farina, "Multi-channel intramuscular and surface EMG decomposition by convolutive blind source separation," *Journal of Neural Engineering*, vol. 13, no. 2, article 026027, 2016.

[33] E. Petersen, H. Buchner, M. Eger, and P. Rostalski, "Convolutive blind source separation of surface EMG measurements of the respiratory muscles," *Biomedizinische Technik*, vol. 62, no. 2, pp. 171–181, 2017.

[34] Z. Huang, B. Fang, X. He, and L. Xia, "Image denoising based on the dyadic wavelet transform and improved threshold," *International Journal of Wavelets, Multiresolution and Information Processing*, vol. 7, no. 3, pp. 269–280, 2009.

[35] M. Ge, G. Cui, and L. Kong, "Mainlobe jamming suppression for distributed radar via joint blind source separation," *IET Radar, Sonar and Navigation*, vol. 13, no. 7, pp. 1189–1199, 2019.

[36] X.-F. Gong, Q.-H. Lin, F.-Y. Cong, and L. De Lathauwer, "Double coupled canonical Polyadic decomposition for joint blind source separation," *IEEE Transactions on Signal Processing*, vol. 66, no. 13, pp. 3475–3490, 2018.

[37] A. Aldhahab and W. B. Mikhael, "Face recognition employing DMWT followed by FastICA," *Circuits, Systems, and Signal Processing*, vol. 37, no. 5, pp. 2045–2073, 2018.

[38] D. G. Fantinato, L. T. Duarte, Y. Deville, R. Attux, C. Jutten, and A. Neves, "A second-order statistics method for blind source separation in post-nonlinear mixtures," *Signal Processing*, vol. 155, pp. 63–72, 2019.

[39] C. Wang, H. Huang, Y. Zhang, and Y. Chen, "Variable learning rate EASI-based adaptive blind source separation in situation of nonstationary source and linear time-varying systems," *Journal of Vibroengineering*, vol. 21, no. 3, pp. 627–638, 2019.

[40] F. Miao, R. Zhao, and X. Wang, "Research on the Fault Feature Extraction Method of Rotor Systems Based on GAW- PSO," *Mathematical Problems in Engineering*, vol. 2020, Article ID 9296720, 10 pages, 2020.

[41] J. H. Lee, H. J. Kwon, and Y. K. Jin, "Numerically efficient implementation of JADE ML algorithm," *Journal of Electromagnetic Waves and Applications*, vol. 22, no. 11-12, pp. 1693–1704, 2008.

[42] F. Miao, R. Zhao, X. Wang, and L. Jia, "A new fault feature extraction method for rotating machinery based on multiple sensors," *Sensors*, vol. 20, no. 6, p. 1713, 2020.

[43] S. Grotas, Y. Yakoby, I. Gera, and T. Routtenberg, "Power systems topology and state estimation by graph blind source separation," *IEEE Transactions on Signal Processing*, vol. 67, no. 8, pp. 2036–2051, 2019.

[44] M. A. Eitner, J. Sirohi, and C. E. Tinney, "Modal parameter estimation of a reduced-scale rocket nozzle using blind source separation," *Measurement Science and Technology*, vol. 30, no. 9, article 095401, 2019.

[45] S. Belaid, J. Hattay, W. Naanaa, and T. Aguili, "A new multiscale framework for convolutive blind source separation," *Signal, Image and Video Processing*, vol. 10, no. 7, pp. 1203–1210, 2016.

[46] F. Miao, R. Zhao, and X. Wang, "A new method of denoising of vibration signal and its application," *Shock and Vibration*, vol. 2020, Article ID 7587840, 8 pages, 2020.

[47] H. Zhao, H. Liu, Y. Jin, X. Dang, and W. Deng, "Feature extraction for data-driven remaining useful life prediction of rolling bearings," *IEEE Transactions on Instrumentation and Measurement*, vol. 70, pp. 1–10, 2021.

[48] M. Lv, C. Zhang, A. Guo, and F. Liu, "A new performance degradation evaluation method integrating PCA, PSR and KELM," *IEEE Access*, vol. 9, pp. 6188–6200, 2021.

[49] X. Cai, H. M. Zhao, S. Shang et al., "An improved quantum-inspired cooperative co-evolution algorithm with mulistrategy and its application," *Expert Systems with Applications*, vol. 171, article 114629, 2021.